



AFRL-RB-WP-TP-2008-3008

TOPOLOGY SYNTHESIS OF DISTRIBUTED ACTUATION SYSTEMS FOR MORPHING WING STRUCTURES (POSTPRINT)

Daisaku Inoyam, Brian P. Sanders, and James J. Joo

**Advanced Structural Concepts Branch
Structures Division**

DECEMBER 2007

Approved for public release; distribution unlimited.

See additional restrictions described on inside pages

STINFO COPY

**AIR FORCE RESEARCH LABORATORY
AIR VEHICLES DIRECTORATE
WRIGHT-PATTERSON AIR FORCE BASE, OH 45433-7542
AIR FORCE MATERIEL COMMAND
UNITED STATES AIR FORCE**

NOTICE AND SIGNATURE PAGE

Using Government drawings, specifications, or other data included in this document for any purpose other than Government procurement does not in any way obligate the U.S. Government. The fact that the Government formulated or supplied the drawings, specifications, or other data does not license the holder or any other person or corporation; or convey any rights or permission to manufacture, use, or sell any patented invention that may relate to them.

This report was cleared for public release by the Air Force Research Laboratory Wright Site (AFRL/WS) Public Affairs Office and is available to the general public, including foreign nationals. Copies may be obtained from the Defense Technical Information Center (DTIC) (<http://www.dtic.mil>).

AFRL-RB-WP-TP-2008-3008 HAS BEEN REVIEWED AND IS APPROVED FOR PUBLICATION IN ACCORDANCE WITH ASSIGNED DISTRIBUTION STATEMENT.

*//Signature//

BRIAN SANDERS
Project Manager

//Signature//

JAMES M. TUSS
Acting Chief
Advanced Structural Concepts Branch

//Signature//

DAVID M. PRATT, Ph.D.
Technical Advisor
Structures Division

This report is published in the interest of scientific and technical information exchange, and its publication does not constitute the Government's approval or disapproval of its ideas or findings.

*Disseminated copies will show “//Signature//” stamped or typed above the signature blocks.

REPORT DOCUMENTATION PAGE

*Form Approved
OMB No. 0704-0188*

The public reporting burden for this collection of information is estimated to average 1 hour per response, including the time for reviewing instructions, searching existing data sources, gathering and maintaining the data needed, and completing and reviewing the collection of information. Send comments regarding this burden estimate or any other aspect of this collection of information, including suggestions for reducing this burden, to Department of Defense, Washington Headquarters Services, Directorate for Information Operations and Reports (0704-0188), 1215 Jefferson Davis Highway, Suite 1204, Arlington, VA 22202-4302. Respondents should be aware that notwithstanding any other provision of law, no person shall be subject to any penalty for failing to comply with a collection of information if it does not display a currently valid OMB control number. **PLEASE DO NOT RETURN YOUR FORM TO THE ABOVE ADDRESS.**

1. REPORT DATE (DD-MM-YY) December 2007			2. REPORT TYPE Journal Article Postprint		3. DATES COVERED (From - To) 31 July 2005 – 31 July 2007					
4. TITLE AND SUBTITLE TOPOLOGY SYNTHESIS OF DISTRIBUTED ACTUATION SYSTEMS FOR MORPHING WING STRUCTURES (POSTPRINT)			5a. CONTRACT NUMBER In-house							
			5b. GRANT NUMBER							
			5c. PROGRAM ELEMENT NUMBER 0601102							
6. AUTHOR(S) Daisaku Inoyam (University of Dayton) Brian P. Sanders (AFRL/RBSA) James J. Joo (University of Dayton Research Institute)			5d. PROJECT NUMBER A03Q							
			5e. TASK NUMBER							
			5f. WORK UNIT NUMBER 0A							
7. PERFORMING ORGANIZATION NAME(S) AND ADDRESS(ES) <table style="width: 100%; border-collapse: collapse;"> <tr> <td style="width: 20%; padding-right: 10px;">University of Dayton Dayton, OH 45469</td> <td>Advanced Structural Concepts Branch, Structures Division Air Force Research Laboratory, Air Vehicles Directorate Wright-Patterson Air Force Base, OH 45433-7542 Air Force Materiel Command United States Air Force</td> </tr> <tr> <td colspan="2" style="border-top: 1px dashed black; padding-top: 5px;">University of Dayton Research Institute Dayton, OH 45469</td> </tr> </table>			University of Dayton Dayton, OH 45469	Advanced Structural Concepts Branch, Structures Division Air Force Research Laboratory, Air Vehicles Directorate Wright-Patterson Air Force Base, OH 45433-7542 Air Force Materiel Command United States Air Force	University of Dayton Research Institute Dayton, OH 45469		8. PERFORMING ORGANIZATION REPORT NUMBER AFRL-RB-WP-TP-2008-3008			
			University of Dayton Dayton, OH 45469	Advanced Structural Concepts Branch, Structures Division Air Force Research Laboratory, Air Vehicles Directorate Wright-Patterson Air Force Base, OH 45433-7542 Air Force Materiel Command United States Air Force						
University of Dayton Research Institute Dayton, OH 45469										
9. SPONSORING/MONITORING AGENCY NAME(S) AND ADDRESS(ES) Air Force Research Laboratory Air Vehicles Directorate Wright-Patterson Air Force Base, OH 45433-7542 Air Force Materiel Command United States Air Force										
10. SPONSORING/MONITORING AGENCY ACRONYM(S) AFRL/RBSA			11. SPONSORING/MONITORING AGENCY REPORT NUMBER(S) AFRL-RB-WP-TP-2008-3008							
			12. DISTRIBUTION/AVAILABILITY STATEMENT Approved for public release; distribution unlimited.							
13. SUPPLEMENTARY NOTES Journal article Journal of Aircraft, Vol. 44, No. 4, July–August 2007. © 2007 American Institute of Aeronautics and Astronautics. The U.S. Government is joint author of this work and has the right to use, modify, reproduce, release, perform, display, or disclose the work. PAO Case Number: WS 07-0675, 09 Jan 2007.										
14. ABSTRACT <p>This paper presents a novel topology optimization methodology for a synthesis of distributed actuation systems with specific applications to morphing air vehicle structures. The main emphasis is placed on the topology optimization problem formulation and the development of computational modeling concepts. The analysis model is developed to meet several important criteria: It must allow a large rigid-body displacement, as well as a variation in planform area, with minimum strain on structural members while retaining acceptable numerical stability for finite element analysis. For demonstration purposes, the in-plane morphing wing model is presented. Topology optimization is performed on a semiground structure with design variables that control the system configuration. In other words, the state of each element in the model is controlled by a corresponding design variable that, in turn, is determined through the optimization process. In effect, the optimization process assigns morphing members as soft elements, nonmorphing load-bearing members as stiff elements, and nonexistent members as “voids.” The optimization process also determines the optimum actuator placement, where each actuator is represented computationally by equal and opposite nodal forces with soft axial stiffness. Sample in-plane morphing problems are solved to demonstrate the potential capability of the methodology.</p>										
15. SUBJECT TERMS										
16. SECURITY CLASSIFICATION OF: a. REPORT Unclassified b. ABSTRACT Unclassified c. THIS PAGE Unclassified			17. LIMITATION OF ABSTRACT: SAR	18. NUMBER OF PAGES 16	19a. NAME OF RESPONSIBLE PERSON (Monitor) Brian Sanders					
					19b. TELEPHONE NUMBER (Include Area Code) N/A					

Topology Synthesis of Distributed Actuation Systems for Morphing Wing Structures

Daisaku Inoyama*

University of Dayton, Dayton, Ohio 45469

Brian P. Sanders†

Air Force Research Laboratory, Wright-Patterson Air Force Base, Ohio 45433

and

James J. Joo‡

University of Dayton Research Institute, Dayton, Ohio 45469

DOI: 10.2514/1.25535

This paper presents a novel topology optimization methodology for a synthesis of distributed actuation systems with specific applications to morphing air vehicle structures. The main emphasis is placed on the topology optimization problem formulation and the development of computational modeling concepts. The analysis model is developed to meet several important criteria: It must allow a large rigid-body displacement, as well as a variation in planform area, with minimum strain on structural members while retaining acceptable numerical stability for finite element analysis. For demonstration purposes, the in-plane morphing wing model is presented. Topology optimization is performed on a semiground structure with design variables that control the system configuration. In other words, the state of each element in the model is controlled by a corresponding design variable that, in turn, is determined through the optimization process. In effect, the optimization process assigns morphing members as soft elements, nonmorphing load-bearing members as stiff elements, and nonexistent members as “voids.” The optimization process also determines the optimum actuator placement, where each actuator is represented computationally by equal and opposite nodal forces with soft axial stiffness. In addition, the configuration of attachments that connect the morphing structure (i.e., morphing wing) to a nonmorphing structure (i.e., fuselage) is determined simultaneously in the same process. Several different optimization problem formulations are investigated to understand their potential benefits in solution quality, as well as meaningfulness of the formulations. Sample in-plane morphing problems are solved to demonstrate the potential capability of the methodology introduced in this paper.

Nomenclature

E_m, E_{\max}	= actual axial stroke length and stroke limit of m th line element
$\mathbf{F}, \mathbf{F}_j^{(0)}, \mathbf{F}_{\text{ext}}$	= global load vector
$\mathbf{K}, \mathbf{K}_i^{(\text{AX})}, \mathbf{K}_i^{(\text{NAX})}$	= rated force vector of j th actuator and external force vector
$\mathbf{K}_i^{(\text{R})}, \mathbf{K}_i^{(\text{NR})}$	= global stiffness matrix
$\mathbf{K}_i^{(\text{S})}, \mathbf{K}_i^{(\text{NS})}$	= axial and nonaxial stiffness of i th line element
K_{skin}	= rotational and nonrotational stiffness of i th joint element
L_1	= sliding and nonsliding stiffness of i th attachment element
L_2	= simulated flexible skin stiffness
N_F	= axial part (subset) of line set
N_L	= nonaxial part (subset) of line set
N_T	= allowable number of fixed attachments
	= total number of line elements in the model
	= total number of target points in the model

Received 31 May 2006; accepted for publication 15 February 2007.
Copyright © 2007 by the American Institute of Aeronautics and Astronautics, Inc. The U.S. Government has a royalty-free license to exercise all rights under the copyright claimed herein for Governmental purposes. All other rights are reserved by the copyright owner. Copies of this paper may be made for personal or internal use, on condition that the copier pay the \$10.00 per-copy fee to the Copyright Clearance Center, Inc., 222 Rosewood Drive, Danvers, MA 01923; include the code 0021-8669/07 \$10.00 in correspondence with the CCC.

*Ph.D. Candidate, Department of Mechanical & Aerospace Engineering. Member AIAA.

†Senior Research Engineer, Air Force Research Laboratory, Air Vehicles Directorate, Advanced Structural Concepts Branch, 2210 8th Street, Building 146. Associate Fellow AIAA.

‡Research Engineer, Aerospace Mechanics Division. Member AIAA.

T, A, J, L, B	= target degree of freedom set, actuator set, joint set, line set, attachment set
\mathbf{U}	= vector of actual displacements
U_i^{TGT}, U_i	= target and actual displacements at i th target degree of freedom
V_{\max}, V_{\min}	= maximum and minimum allowable volume
W_i	= weight/scaling constant for i th objective term
β, p, q, α	= penalty constants for joint, line, actuator, and attachment variables
ε_{\max}	= maximum allowable target point error
ρ, ρ_j	= vector of design variables and its i th components in the set
ρ_{\min}	= minimum value of design variables in line sets (i.e., L_1 and L_2)

I. Introduction

CONVENTIONAL air vehicles are designed and optimized for specific flight conditions and profiles. When the vehicle maneuvers away from these design points, the performance often declines dramatically. Although the ability to adapt the air vehicle shape to attain an optimum flight performance is highly desirable, the conventional fixed wing design is technically limited, if not impossible, to accomplish this revolutionary performance objective. Therefore, major research efforts (see, for example, [1,2]) have been spurred recently to develop concepts, methodology, and ideas to efficiently morph air vehicle geometry into optimum shapes according to various flight environments. In addition to developing the enabling technology, new design approaches are also required to uncover morphing wing concepts.

Recent studies by Maute et al. [3,4] on the morphing wing mechanism illustrated that the topology optimization method has the potential to be applied to efficiently determine the optimum

mechanism topology of a morphing air vehicle wing. One of the investigations presents a material-based topology optimization methodology for the mechanism design of an in-plane morphing wing [3]. The study involves single- and triple-layer wing models to observe the artificial stiffness of the model and its effect on the mechanism topology. In addition, the effect of skin stiffness on the mechanism topology is demonstrated. Considerations and analyses are given on different problem formulations, including output energy maximization and shape matching. The globally convergent version of method of moving asymptotes (GCMMA) is used to solve the in-plane morphing problem. Although Maute established the foundation to the work being introduced here, no considerations are given on a combined actuator placement/topology optimization problem, as well as the determination of wing-fuselage attachments.

A research effort by Lu and Kota on the mechanism topology demonstrated a synthesis of a compliant mechanism for morphing structural shapes using simultaneous topology and dimensional optimizations [5]. The study involves the genetic algorithm (GA) to simultaneously determine mechanism topology and dimensions by minimizing the coordinate errors between active and target points on shape changing boundaries. Several problem formulations are presented in their work, including pointwise least-square error and curvewise Fourier transform (FT, DFT, and FFT) error minimization problems. In addition, analyses and considerations are given on the variation of mechanism topology due to these formulations. Although the study has shown the versatility of topology optimization as applied to mechanism design, no considerations are given on actuator placement.

Recently, several studies were conducted on the distributed actuation to control the performance of aeroelastic air vehicles [6–9]. One of the notable investigations by Gern et al. demonstrates the possible advantage of a morphing wing with distributed actuators, especially at the high speed [6]. The research is conducted on the equivalent plate model of generic uninhabited combat air vehicle (UCAV). The aerodynamics analysis involves the vortex lattice method together with Prandtl-Glauert compressibility correction. In the analysis, fully coupled static aeroelasticity is considered and the comparison of flexible roll performance between morphing and conventional air vehicles is made. Besides its potential in system robustness and redundancy, the research has shown that distributed actuators may efficiently control wing morphing while achieving vehicle performance equivalent or superior to conventional control systems. Although the investigation addressed the actuator energy requirement, it places no considerations on the impact of actuator placement or mechanism topology. In addition, the study only involved the airfoil morphing and no large-scale planform morphing is considered.

Several studies involving the optimal actuator placement were conducted in recent years [10–12]. One investigation demonstrates the minimization of the number of discrete actuators while achieving a specified flight performance [10]. The study uses the GA to solve the actuator placement optimization problem and explained the characteristics of GA as applied to such problems. Moreover, researchers introduce an innovative method of aerodynamically defining an actuator by the source-sink combination. It is an excellent approach, but the analysis model consists solely of rigid aerodynamic panels. Therefore, it lacks the effect of elastic and rigid-body structural deformations on the actuator placement.

Although these past investigations [1–15] pose an excellent illustration of the basic pieces of design for morphing structures, no work has been conducted on the combined system of real interest. Therefore, the main emphasis of this paper is placed on the development of reliable analysis model and the formulations of combined multidisciplinary topology optimization problems that are excluded from the past investigations. The investigation is conducted on the combination of disciplines including mechanization, actuator placement, attachment determination, and topology optimization. Several different formulations are introduced in this paper: The first formulation involves the multi-objective function with total actuator utilization and shape-matching error terms. The other formulations involve the choice of either actuator utilization or shape matching as

objective and the one not included in the objective function to be treated as constraints. In addition, the potential benefits of combined or sequentially executed formulations are discussed in some detail. It is expected that the research will provide an important “first step” for the topology synthesis of distributed actuation system design for morphing air vehicles.

II. General Procedure and Technical Approach

A. Analysis Model Description

The in-plane morphing wing model introduced here is a semiground structure consisting of joint, line, and attachment elements as shown in Fig. 1. Although it is understood that more reliable results can probably be obtained from full or other configurations of semiground structure, this particular form is chosen for simplicity and to minimize computational efforts. To determine the appropriate displacement boundary condition at the wing root that attaches to a nonmorphing fuselage, attachment elements are placed on each point along the inner edge of the model. Aerodynamic drag loads are simulated by in-plane nodal forces at the wing leading edge. Out-of-plane aerodynamic pressures are not considered in this investigation, although it is a subject for future research.

Each line element assumes an appropriate configuration depending on the value of design variables that are determined by the optimization process, which is discussed later. Line elements in the model can be frames, trusses, telescoping members, or actuators as shown in Fig. 2. Frame elements are conventional finite elements with axial and bending stiffness. Truss elements only possess axial stiffness. Telescoping members are classified into two categories, active and inactive. Inactive telescopes are prismatic elements that have “very low” axial stiffness with beam bending stiffness and are not capable of delivering an actuation force. Whenever a telescoping member has an associated actuation force, the element is classified as an active telescope. An actuator is simply an element with equal and opposite nodal forces at its nodes. In other words, the primary difference between a simple actuator and an active telescope is that the latter one is capable of carrying bending loads internally. Both telescoping members and actuators have axial stroke limits that prohibit them from extending more than a predefined length, thereby preventing these elements from having unrealistically large strokes. In addition, actuator forces are limited to a certain predefined value. Whenever very low stiffness is present in all degrees of freedom, the element is considered as structurally or mechanically non-contributing and selected to be nonexistent or void.

Joint elements can be classified into the following types: revolute, compliant, or semirigid, as shown in Fig. 3. These joints are analogous to rotational springs with variable rotational stiffness. Revolute joints can be considered as rotating hinges simulated by very low rotational stiffness and “very high” stiffness in all other directions. Conversely, semirigid joints have very high stiffness in

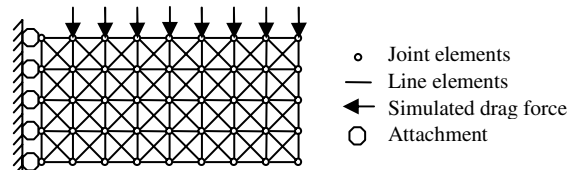


Fig. 1 Analysis model.

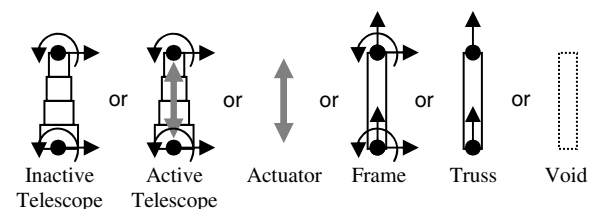


Fig. 2 Line element configurations.



Fig. 3 Joint element configurations.



Fig. 4 Attachment element configurations.

rotational and all other directions. Compliant joints have intermediate rotational stiffness that can be physically interpreted as friction joints or high-strain joints. In addition to motions around these defined joints, rotations about truss elements are also possible as in the case of implicitly defined pinned joints in truss structures.

Among several possible configurations for an attachment element, two primary ones, as shown in Fig. 4, are considered in the model presented here. The attachments are modeled as linear springs with variable translational stiffness. The sliding boundary condition allows corresponding attachments to slide in a single translational direction along fuselage, which is numerically represented by very low stiffness in a sliding direction and very high stiffness in other directions. The fixed boundary condition prohibits any motions by very high stiffness in entire degrees of freedom.

The words very low and very high are relative to the full stiffness of a frame element. Therefore, rigid-body motions are a result of relatively “soft” elements and, at the same time, structural strains are carried to the load resisting structure through relatively “stiff” elements. Evidently, very low and very high values must be chosen carefully to ensure numerical stability.

In addition to line, joint, and attachment elements, the model contains flexible skin elements. Because reliable representation of a flexible morphing vehicle skin is not available at the moment, four-node rectangular elements with very compliant membrane stiffness are applied over each “cell” to represent the flexible skin. Although importance of reliable skin model is well understood, the “pillowing” effect that arises from out-of-plane pressure loading is not a concern for the problem presented in this paper, and therefore, such a simple representation of flexible skin is considered to be sufficient.

This paper deals only with linear finite element method (FEM) to keep the analysis at the conceptual level, but the model discussed in this section should be equally applicable to geometrically/material nonlinear finite element cases, where stiffness and force boundary conditions are function of displacement, with significant increase in computational costs.

B. Optimization Problem Formulations

Three different optimization problem formulations are investigated in this paper. The first formulation involves a multi-objective function to minimize shape-matching error and actuator utilization simultaneously. The second and third formulations consist of a single objective with extra constraints to avoid notoriously weighting-dependent multi-objective formulation. Additionally, the sequential combinations of these formulations are considered.

1. Multiple-Objective Minimization

The multi-objective formulation involves an objective function with weighted sum of shape-matching error and actuator utilization terms. The constraints include the satisfaction of the static equilibrium condition, line element stroke limit, and volume limit. Although the multi-objective formulation is often discredited as unreliable, potential benefits of this formulation are not to be discounted here. The approach can be stated as follows:

Minimize:

$$f_0 = W_1 \sum_{i \in I} [U_i^{\text{TGT}} - U(\rho)_i]^2 + W_2 \sum_{j \in A} \rho_j^2 \quad (1)$$

Subject to:

$$f_{\text{eq}} = \mathbf{K}\mathbf{U} - \mathbf{F} = \mathbf{0} \quad (2)$$

$$f_m = E_m^2 - E_{\max}^2 \leq 0 \quad m = 1, \dots, N_L \quad (3)$$

$$f_{+V} = \sum_{i \in L1} \rho_i + \sum_{i \in L2} \rho_i - V_{\max} \leq 0 \quad (4)$$

$$f_{-V} = -\sum_{i \in L1} \rho_i - \sum_{i \in L2} \rho_i + V_{\min} \leq 0 \quad (5)$$

$$f_F = \sum_{i \in B} \rho_i - N_F \leq 0 \quad (6)$$

$$\rho_{\min} \leq \rho_i \leq 1.0 \quad i \in J, L1, L2, B \quad (7)$$

$$-1.0 \leq \rho_j \leq 1.0 \quad j \in A \quad (8)$$

where

$$\begin{aligned} \mathbf{K} = & \sum_{i \in J} (\rho_i^\beta \mathbf{K}_i^{(R)} + \mathbf{K}_i^{(\text{NR})}) + \sum_{i \in L1} (\rho_i^p \mathbf{K}_i^{(\text{AX})}) + \sum_{i \in L2} (\rho_i^p \mathbf{K}_i^{(\text{NAX})}) \\ & + \sum_{i \in B} (\rho_i^\alpha \mathbf{K}_i^{(S)} + \mathbf{K}_i^{(\text{NS})}) + \mathbf{K}_{\text{skin}} \end{aligned} \quad (9)$$

$$\mathbf{F} = \sum_{j \in A} \rho_j^q \mathbf{F}_j^0 + \mathbf{F}_{\text{ext}} \quad (10)$$

Clearly, f_0 is the multi-objective function with shape-matching and actuator utilization terms. The static equilibrium condition is f_{eq} and it must be satisfied identically at every iterations. The design variables ρ_i control the corresponding stiffness of each elements as indicated in (9). Axial stroke constraints f_m for line elements are expressed as the sum of the differences of squares of actual stroke length and maximum allowable stroke length. The “volume” range constraints (f_{+V} and f_{-V}) do not represent the actual volume of the structure, but they instead correspond to the allowable range of the sum of line element design variables, where V_{\max} is the upper limit and V_{\min} is the lower limit. The attachment constraint f_F defines the maximum allowable number of fixed attachments to a nonmorphing structure or fuselage. The actuator utilization is the second term in the objective function, which is expressed as the sum of squared actuator variables.

The first term of the objective function is a shape-matching objective that is ideally zero when the actual displacements match the target displacements at the target points. In many cases, this type of pointwise shape matching may not be the best representation as it “forces” predefined target points in the structure to move to certain assigned locations. Instead, the target shape can be represented as a function, such as a spline or polynomial function, and let points along morphing boundary to position along a target function as shown in Fig. 5. The functionwise shape-matching term can be written as the sum of squared differences of actual and target shape function coefficients:

$$\begin{aligned} f_{\text{shape}} = & [A(\mathbf{U}) - A_{\text{TGT}}]^2 + [B(\mathbf{U}) - B_{\text{TGT}}]^2 \\ & + [C(\mathbf{U}) - C_{\text{TGT}}]^2 + \dots \end{aligned} \quad (11)$$

where actual shape function is $S(A, B, C, \dots)$ and target shape function is $T(A_{\text{TGT}}, B_{\text{TGT}}, C_{\text{TGT}}, \dots)$.

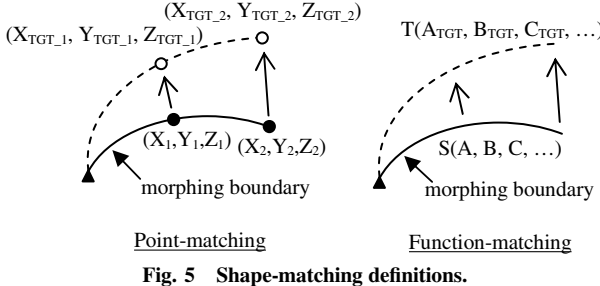


Fig. 5 Shape-matching definitions.

For the sake of simplicity and to minimize computational costs, pointwise matching is used in this investigation. Here, sensitivities of the objective function with respect to design variables are computed by the adjoint variable method, where equilibrium conditions are satisfied a priori in computation as follows:

$$\frac{\partial f_0}{\partial \rho_e} = \begin{cases} -2W_1\beta\rho_e^{\beta-1}\sum_{i\in T}\left[\left(U_i^{TGT} - U_i\right)\lambda_i^T \mathbf{K}_e^{(R)} \mathbf{U}\right] & e \in J \\ -2W_1p\rho_e^{p-1}\sum_{i\in T}\left[\left(U_i^{TGT} - U_i\right)\lambda_i^T \mathbf{K}_e^{(AX)} \mathbf{U}\right] & e \in L1 \\ -2W_1p\rho_e^{\alpha-1}\sum_{i\in T}\left[\left(U_i^{TGT} - U_i\right)\lambda_i^T \mathbf{K}_e^{(NAX)} \mathbf{U}\right] & e \in L2 \\ -2W_1\alpha\rho_e^{\alpha-1}\sum_{i\in T}\left[\left(U_i^{TGT} - U_i\right)\lambda_i^T \mathbf{K}_e^{(S)} \mathbf{U}\right] & e \in B \\ 2W_1q\rho_e^{q-1}\sum_{i\in T}\left[\left(U_i^{TGT} - U_i\right)\lambda_i^T \mathbf{F}_e\right] + 2W_2\rho_e & e \in A \end{cases} \quad (12)$$

where λ_i is the solution to adjoint problem for i th target degree of freedom:

$$\mathbf{K}\lambda_i = -\mathbf{l}_i \quad (13)$$

and \mathbf{l}_i is the vector with 1 in i th component and 0 in all other components as defined by

$$U_i = \mathbf{l}_i^T \mathbf{U} \quad (14)$$

Similarly, sensitivities of constraint functions with respect to design variables can be written as follows:

$$\frac{\partial f_m}{\partial \rho_e} = \begin{cases} 2\beta\rho_e^{\beta-1}\Psi_m^T \mathbf{U} \eta_m^T \mathbf{K}_e^{(R)} \mathbf{U} & e \in J \\ 2p\rho_e^{p-1}\Psi_m^T \mathbf{U} \eta_m^T \mathbf{K}_e^{(AX)} \mathbf{U} & e \in L1 \\ 2p\rho_e^{p-1}\Psi_m^T \mathbf{U} \eta_m^T \mathbf{K}_e^{(NAX)} \mathbf{U} & e \in L2 \\ 2\alpha\rho_e^{\alpha-1}\Psi_m^T \mathbf{U} \eta_m^T \mathbf{K}_e^{(S)} \mathbf{U} & e \in B \\ -2q\rho_e^{q-1}\Psi_m^T \mathbf{U} \eta_m^T \mathbf{F}_e^0 & e \in A \end{cases} \quad (15)$$

$$\frac{\partial f_{+V}}{\partial \rho_e} = \begin{cases} 1.0 & e \in L \\ 0.0 & e \notin L \end{cases} \quad \frac{\partial f_{-V}}{\partial \rho_e} = \begin{cases} -1.0 & e \in L \\ 0.0 & e \notin L \end{cases} \quad (16)$$

$$\frac{\partial f_F}{\partial \rho_e} = \begin{cases} 1.0 & e \in B \\ 0.0 & e \notin B \end{cases} \quad (17)$$

η_m is the solution to adjoint problem for m th stroke limit constraint:

$$\mathbf{K}\eta_m = -\Psi_m \quad (18)$$

where Ψ_m is the vector of positive and negative of sine and cosine of m th line element coordinate as defined by

$$E_m = \Psi_m^T \mathbf{U} \quad (19)$$

Depending on optimization techniques, an appropriate scaling scheme can be applied to the preceding formulation to make the problem more suitable or numerically stable. The obvious disadvantage of this formulation is its dependency on objective

weighting constants. Therefore, it is imperative to investigate other formulations that do not contain multiple objectives.

2. Actuator Utilization Minimization with Shape-Matching Constraints

This formulation has a single objective and an extra shape-matching constraint. Because the shape matching can be considered as a requirement, instead of achievement, the following minimization problem can be solved along with constraints (2–8):

Minimize:

$$f_0 = \sum_{j \in A} \rho_j^2 \quad (20)$$

Subject to:

$$f_n = \left(U_n^{TGT} - U_n \right)^2 - \varepsilon_{max}^2 \leq 0 \quad n = 1, \dots, N_T \quad (21)$$

where f_0 is the objective function that aims to minimize the total squared actuator utilization and f_n is the shape-matching constraint for n th target point. This formulation has a compact objective sensitivity:

$$\frac{\partial f_0}{\partial \rho_e} = \begin{cases} 2.0\rho_e & e \in A \\ 0.0 & e \notin A \end{cases} \quad (22)$$

The sensitivities of constraint functions are determined using the adjoint method:

$$\frac{\partial f_n}{\partial \rho_e} = \begin{cases} -2\beta\rho_e^{\beta-1}\left(U_n^{TGT} - U_n\right)\lambda_n^T \mathbf{K}_e^{(R)} \mathbf{U} & e \in J \\ -2p\rho_e^{p-1}\left(U_n^{TGT} - U_n\right)\lambda_n^T \mathbf{K}_e^{(AX)} \mathbf{U} & e \in L1 \\ -2p\rho_e^{p-1}\left(U_n^{TGT} - U_n\right)\lambda_n^T \mathbf{K}_e^{(NAX)} \mathbf{U} & e \in L2 \\ -2\alpha\rho_e^{\alpha-1}\left(U_n^{TGT} - U_n\right)\lambda_n^T \mathbf{K}_e^{(S)} \mathbf{U} & e \in B \\ 2q\rho_e^{q-1}\left(U_n^{TGT} - U_n\right)\lambda_n^T \mathbf{F}_e^0 & e \in A \end{cases} \quad (23)$$

All other constraint sensitivities and the solutions to adjoint problems are identical to those of the multi-objective formulation.

This formulation has the disadvantage in the starting condition due to the fact that the optimization process must start with large shape constraint violation. Therefore, to solve this problem, optimization techniques must include means to treat large constraint violations. In such optimization techniques, constraint violation minimization may be performed before the minimization of supplied objective until the satisfaction of all violated constraints is achieved.

3. Shape Error Minimization with Actuator Utilization Constraints

Another formulation that is worth investigating involves an objective function to achieve minimum shape-matching error and constraints to maintain the total squared actuator utilization within a defined range. This optimization problem, in conjunction with constraints (2–8), can be written as follows:

Minimize:

$$f_0 = \sum_{i \in T} \left[U_i^{TGT} - U(\rho)_i \right]^2 \quad (24)$$

Subject to:

$$F_{+A} = \sum_{j \in A} \rho_j^2 - A_{max} \leq 0 \quad (25)$$

$$F_{-A} = -\sum_{j \in A} \rho_j^2 + A_{min} \leq 0 \quad (26)$$

where the total squared actuator utilization constraints (F_{+A} and F_{-A}) are defined as the maximum and minimum of the sum of squares of actuator variables. A_{max} and A_{min} are constants that represent the

allowable actuator utilization range. In addition, it should be noted that “utilization” does not indicate the “quantity” of actuators because the square of actuator variables are not necessarily discrete zero or one as they are often desired to be continuous in nature. In this formulation, the objective sensitivities are determined as in the preceding cases:

$$\frac{\partial f_0}{\partial \rho_e} = 2q\rho_e^{q-1} \sum_{i \in I} \left[(U_i^{\text{TGT}} - U_i) \lambda_i^T \mathbf{F}_e^0 \right] \quad e \in A \quad (27)$$

The sensitivities of constraint functions are identical to those of the multi-objective case, except that the formulation has additional actuator constraint sensitivities:

$$\frac{\partial f_{+A}}{\partial \rho_e} = \begin{cases} 2.0\rho_e & e \in A \\ 0.0 & e \notin A \end{cases} \quad \frac{\partial f_{-A}}{\partial \rho_e} = \begin{cases} -2.0\rho_e & e \in A \\ 0.0 & e \notin A \end{cases} \quad (28)$$

Again, the solutions to adjoint problems are identical to those of preceding formulations.

4. Combination of Formulations

Each formulation has advantages and disadvantages over one another. As mentioned, the multi-objective formulation has a disadvantage of being dependent on weighting constants. The actuator minimization formulation has large shape constraint violation at the initial iterations. Moreover, the total squared actuator utilization value must be known and assigned a priori in case of the shape error minimization formulation. Therefore, it may be beneficial to incorporate the process to execute the formulations in sequential fashion to cover the disadvantage of one formulation by the advantage of another formulation. For instance, one can consider the two-step process involving the multi-objective or shape error minimization formulation followed by the actuator utilization formulation, thereby avoiding the large shape constraint violation while the initial formulation is in effect. As soon as the shape error becomes small enough that target points are within the maximum allowable target point error or ε_{max} , one can change the formulation to that of actuator utilization minimization. At that moment, the balance between weighting constants or the assigned actuator value, whichever applicable, becomes irrelevant to the solution and the optimization process would find an optimal utilization of actuators while maintaining the acceptable target shape.

In terms of formulation definitions, the shape error minimization formulation may favor the “bull’s eye” target shape satisfaction because its sole objective is to minimize the shape error. The multi-objective formulation can consider both shape and actuator utilization simultaneously, though the shape objective should generally dominate the process at initial iterations in the process. The actuator minimization formulation may be able to find an optimum actuator utilization while maintaining the acceptable shape, but its large constraint violation at the initial stage in the process may prevent the solution from converging to the desired optimum, because the procedure to correct the constraint violation may not be reliable. The combined formulation may possess both the shape precision of multi-objective or shape error minimization formulations and the shape relaxation characteristics of actuator minimization formulation as shown in Fig. 6.

C. Computational Procedures

The analysis involves several components. The mesh generator and preprocessor define the initial parameters and create the model consisting of a ground structure with attachment, joint, and line elements. Finite element analysis is performed within the optimization process to evaluate objective and constraint functions. To solve this multidisciplinary optimization problem, GCMMA [16,17] is used in the investigation. In each inner and outer iteration of GCMMA, convex subproblems are generated and solved by the primal-dual interior point approach. In addition, the conservativeness of each subproblem generated is monitored and adjusted as necessary. The general flow of the program is depicted in the Fig. 7.

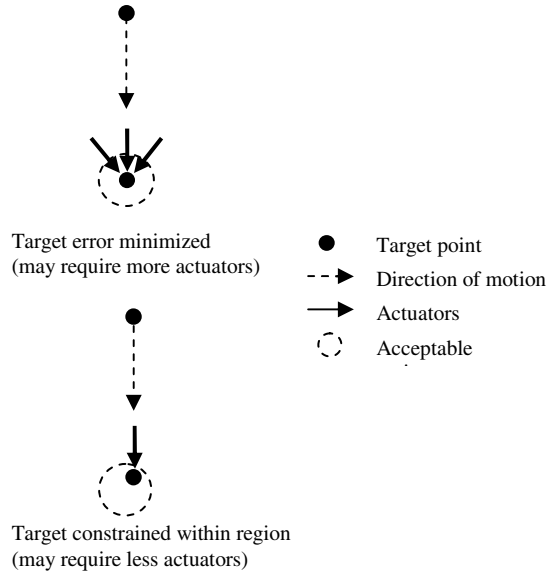


Fig. 6 Effect of target definitions.

The convergence is attained when the objective value is sufficiently small without any constraint violations.

III. Sample In-Plane Problems and Results

The sample problem provided here includes the main characteristics of an in-plane morphing wing as shown in Fig. 8. First, it involves a large rigid-body rotation that results from a sweeping motion of the wing. In addition, it includes a dramatic variation in a planform shape with 37.5% increase in wing area. The initial configuration of the model is a rectangular semiground structure of 4×4 cells with evenly distributed initial design variables. The outer line of the structure is assigned as a morphing boundary, which ideally matches the target boundary shape after the optimization process. Solutions are obtained using all problem formulations introduced in the preceding sections. For all cases, predefined parameters are assigned identically to facilitate the valid comparison.

The physical and material properties of the full frame element are chosen to resemble a frame with 1×1 in. square cross section that is made of the common aluminum alloy. The beam and truss elements are decompositions of the frame structure with the same physical and material properties. Consequently, the elasticity modulus of these line elements is allowed to vary between $1\text{e}7$ and $1\text{e}-5$ psi. The membrane stiffness of skin elements is selected to be 100 psi with Poisson’s ratio of 0.3 and a thickness of 0.1 in. Although one may argue that the skin stiffness is excessively low, the artificial shear stiffness that may be present in the linear rectangular element must be considered. As noted, further investigations are required to model the flexible skin more effectively.

A. Multi-Objective Case

For this particular problem, the desired relative volume parameter is selected to be 0.25 or below. This relative volume parameter value prevents the total number of structural elements (i.e., frame, telescope, truss) in the converged solution to exceed 50% of the initial volume. As a consequence, all line element design variables are initially assigned at or below this value to avoid a volume constraint violation. The initial value of actuator variables are somewhat arbitrary unless the utilization value is constrained to fall within a specific range, but some initial values may be better than others as in any other optimization problems. The weighting constant for the actuator minimization term is chosen not to be excessively underweighted because the shape-matching term tends to dominate in initial iterations.

In Figs. 9a and 9b, it is clearly visible that the initial wing design (semiground structure in Fig. 8) that consists of 72 line elements was

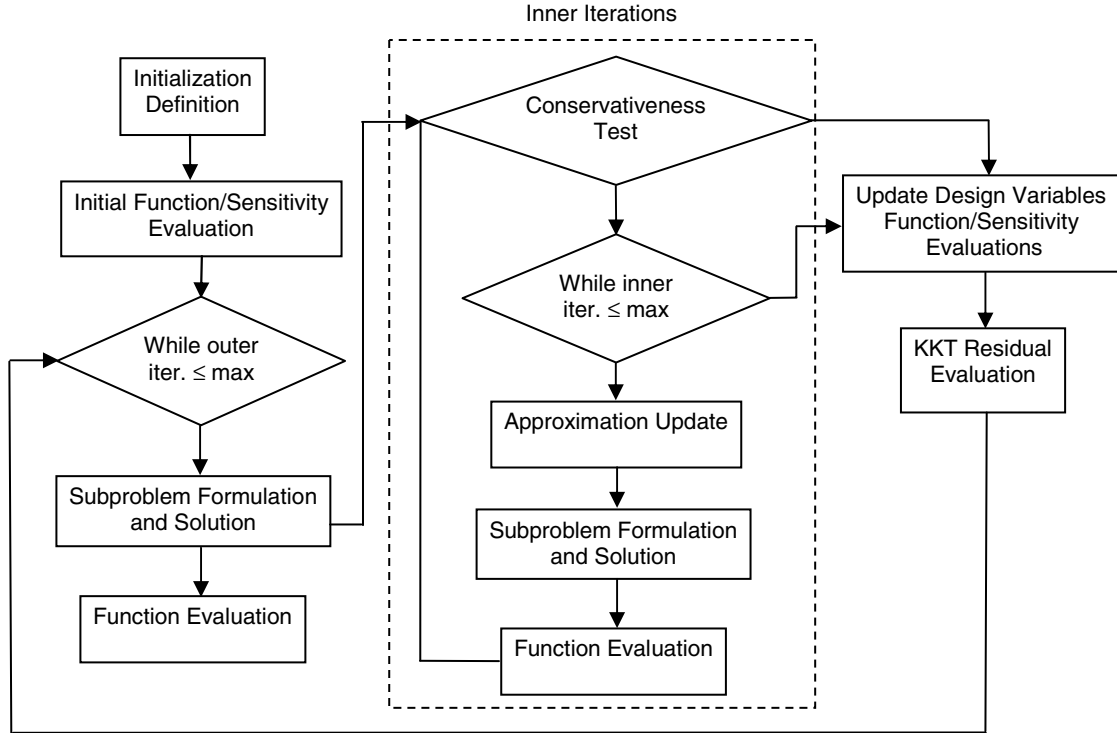


Fig. 7 Optimization process flow chart.

reduced to a more compact morphing structure. In addition, the optimization process determined 17 actuator positions (3 pull and 14 push) among 72 possible locations. The solution only contains truss elements, though capabilities to select beam or frame elements with bending stiffness are provided in the program. This is an understandable outcome, especially for the in-plane problem selected for this demonstration, because the best direction to transfer or resist loads for any bar-type elements is along its axial coordinate. The configuration of the joint elements, in this all-truss solution, is through the rotational characteristics of truss element as described in Sec. II.A (this is not necessarily the case for other problems with different target shape and loading conditions). The figures also reveal that larger accumulations of structural components in the leading-edge section and lesser in the trailing-edge section. One can hypothesize that this structural buildup at the leading edge is essential to handle the simulated external loads and to transform the loads into the sweeping moment to cause a large rotational wing motion, minimizing the use of actuators for the purpose. Because the aft section lacks the assistance of external loads, it requires actuators

to cause small shape changes and expand the wing area. In addition, an actuator appears in somewhat an unorthodox location, where an actuator pushes onto the wing tip against the flexible skin. The cause of this phenomenon is probably inherent to the optimization process and correlated to the modeling deficiency of a flexible skin. As the structure at the leading edge sweeps backward, it compresses the skin and creates a "fishtail" shape at the wing tip. The ideal skin design should not cause any motions that require independent actuator to counteract. Instead, the flexible skin should flow naturally into the target shape as it deforms. Although this is clearly an undesirable characteristic of the flexible skin model, the program strives to correct the situation as the shape error minimization is one of its main objectives. For this particular instance, the optimization process

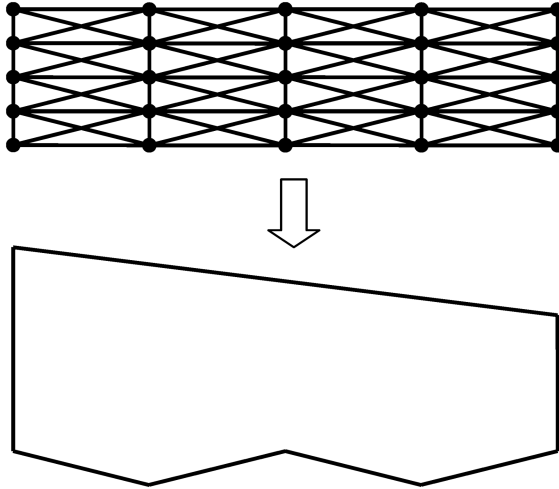
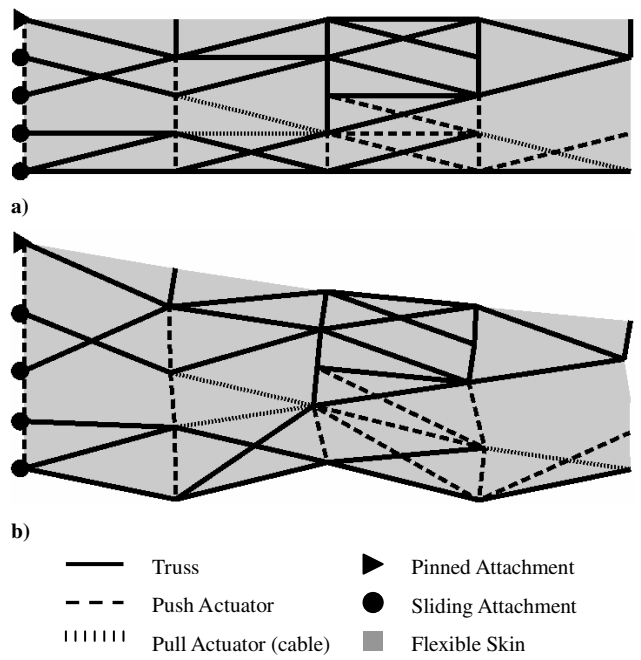


Fig. 8 Sample problem definition.



6 Fig. 9 a) Position 1, b) position 2 for the multiple-objective formulation.

outweighed the shape match and determined that it is more beneficial to use actuators to correct this shape error. The displacement behavior of the skin can possibly be modified to correct the situation. The total absolute actuator utilization (i.e., sum of absolute value of actuator design variables) for the case was found to be 4.267 and the total normalized shape error (i.e., total shape error/total target shape change) was 0.0784. At the attachment section, it is clearly visible that the optimization process determined the proper configuration to accommodate the desired shape change. In terms of accuracy and reliability of this result, one can observe that some parts of the structure may not be physically correct to make such motions. One main reason for this defect can be traced to linear FEM used in this large-displacement analysis.

B. Actuator Utilization Minimization with Shape Constraint Case

Because the shape-matching is treated as constraints for this particular case, the problem essentially turns into the combination of constraint violation minimization and actuator minimization at initial iterations in the process. Therefore, this problem cannot be solved by optimization schemes that do not incorporate constraint violation measures. Because constraint violations are generally penalized severely, it is expected that the initial phase of the optimization process would be dominated by the constraint violation minimization. Consequently, the magnitude of constraint violation penalty may make a significant difference in the solution. Here, the initial condition is identical to that of the multi-objective case.

Figures 10a and 10b reveal that the shape objective was met quite acceptably as in the last case. Although the normalized total shape error of 0.1589 is somewhat higher than the last case, the resultant shape seems acceptable. This shape error is explicable as the shape matching is included in constraints with pointwise relaxation that allow each target point to have the maximum normalized displacement error of approximately 0.015. For that reason, one may notice that the fishtail effect at the wing tip is no longer corrected by an actuator as the formulation is essentially more tolerant of shape errors. Consequently, the total absolute actuator utilization value was smaller for this case as the optimization process did not have to sacrifice large actuator utilization for the relatively insignificant shape accuracy. Additional computations revealed that the actuator work ratio of multi-objective result to the present result is approximately 1.0 to 0.793, indicating that the present result is approximately 21% superior in terms of actuator work. Furthermore,

structural topologies, as well as joint configurations, for both cases are fundamentally similar with rigid structures at the leading edge. The attachment configuration was determined to be the same as the last case.

Despite the fact that the actuator minimization formulation provided a superior result for this particular problem, it is not indicative that the formulation will work better for other problems. Certainly, one can imagine the situation in which shape accuracy is significantly more critical than the amount of actuator utilization. Moreover, this formulation, as mentioned, has very large shape constraint violations at the initial phase of optimization process and it is often difficult to attain convergence.

C. Shape Error Minimization with Actuator Constraint Case

For this case, the assumption must be made that the desired actuator utilization value is known a priori. To facilitate the valid comparison, the total squared actuator value obtained from the preceding case was applied. For instance, the multi-objective case provided the value of approximately 1.0. The problem was solved with the constraint to match this actuator parameter along with conditions identical to those of multi-objective case.

As one can observe from Figs. 11a and 11b, the multi-objective case and the present case provided a strikingly similar result. This similarity may be plausible as these two formulations share the similar objective and the optimizations were performed with nearly identical conditions and parameters. The total absolute actuator utilization was 4.410, which is only fractionally different from that of multi-objective case. One may notice that the total absolute actuator value is different from that of multi-objective case, though both cases have the same total squared actuator utilization value. This is due to the difference in definition between "sum of squares" and "sum of absolute values." In other words, the same total squared actuator utilization (sum of squares) does not necessarily imply the same total absolute actuator utilization (sum of absolute values). The total normalized shape error for the case was 0.0802, indicating that the shape objective was met rather precisely. The work ratio of the multi-objective case to the present case was approximately 0.956 to 1.0, which can be considered as a negligible difference. Again, this is not a surprising conclusion because dominant actuators for both cases are positioned in the similar locations to achieve the same shape change.

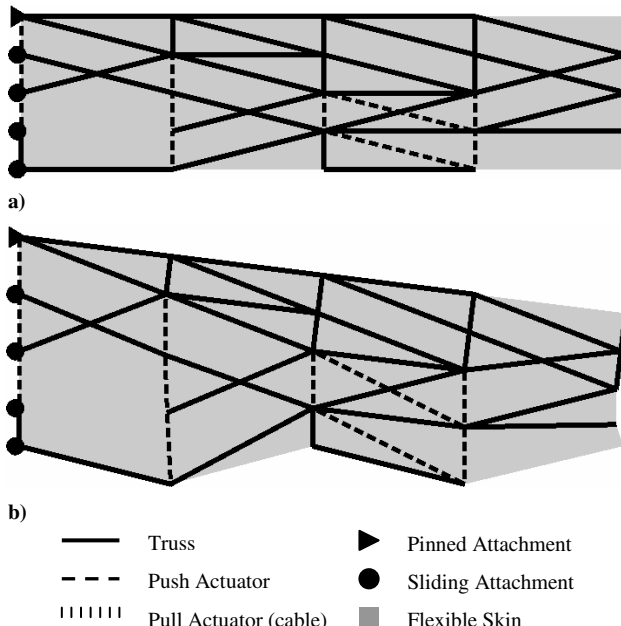


Fig. 10 a) Position 1, b) position 2 for the actuator minimization formulation.

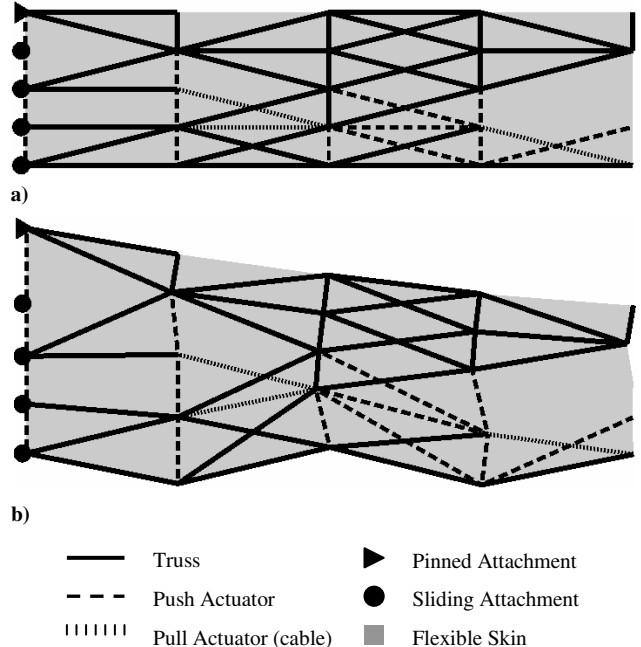


Fig. 11 a) Position 1, b) position 2 for the shape error minimization formulation.

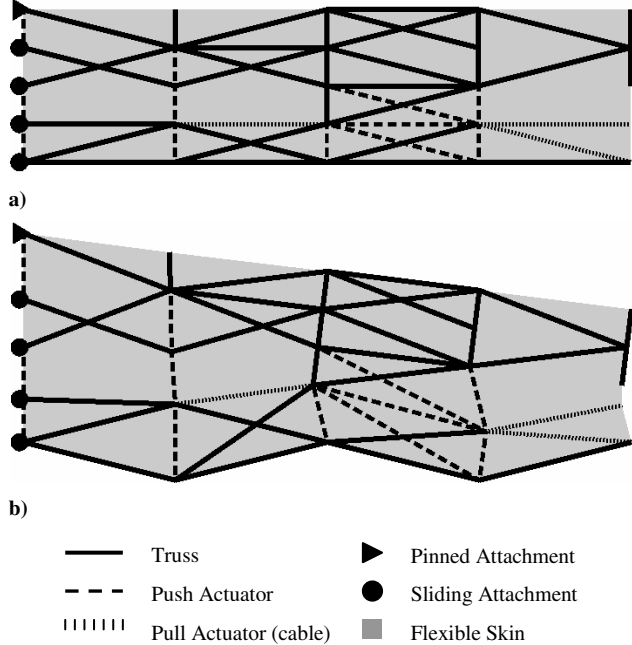


Fig. 12 a) Position 1, b) position 2 for the combination of multi-objective and actuator formulations.

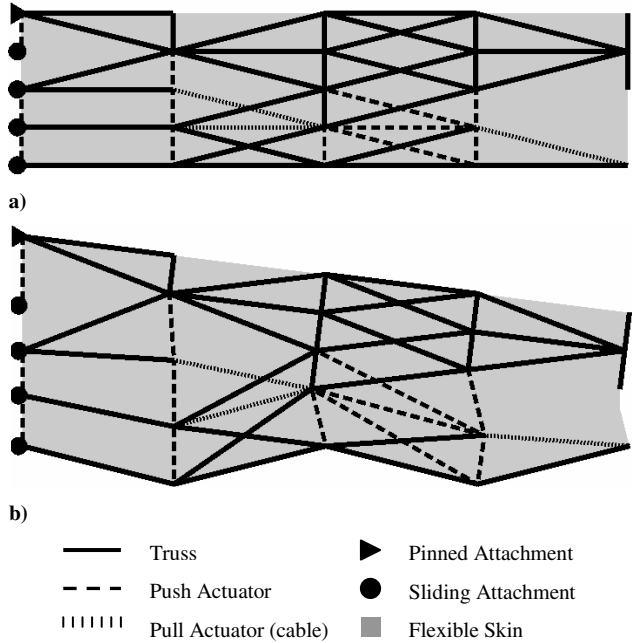


Fig. 13 a) Position 1, b) position 2 for the combination of shape error and actuator formulations.

D. Combinations of Formulations

In this section, the potential benefit of using a combination scheme is demonstrated. The solution from multi-objective case was applied to the actuator minimization formulation. Figures 12a and 12b reveal

that the actuator minimization reduced the actuator usage without changing the shape or the topology of the structure significantly. Otherwise stated, the actuator minimization followed by the solution of multi-objective case may result in a favorable “tightening” effect on the actuator utilization, assuming that the slight loss in the shape accuracy is not a major concern. The total normalized shape error was 0.1525 with the total absolute actuator utilization of 3.8198, indicating that the actuator requirement was indeed reduced at the expense of shape preciseness. The total actuator work was computed to be 13.34% less than that of the noncombination case. At the wing tip, the fishtail effect is clearly visible as the latter formulation was set to be more resilient to shape errors to reduce the actuator utilization.

The same process was applied to the shape error minimization solution from Sec. III.C. Figures 13a and 13b illustrate the similar tightening effect as that of the preceding case. The total normalized shape error and absolute actuator utilization were 0.1508 and 3.9103, respectively. The total actuator work was reduced 13.09% compared to the noncombination case. One may notice that an actuator to hold the fishtail effect has vanished and the fishtail effect is clearly visible for the same reason as the last case.

IV. Conclusions

In this paper, the topology optimization methodology for the determination of actuation system configuration for in-plane morphing wing was introduced. The modeling concept incorporates a variety of elements (i.e., frame, truss, telescopes, actuator, attachment, and joint) to effectively produce rigid-body shape change in wing planform. Moreover, several optimization problem formulations were discussed and investigated to observe the formulation dependency on numerical solutions, as well as meaningfulness of the formulation itself. The first formulation involves the multi-objective function. Other cases are single-objective formulation with extra constraints. The combination of formulations was also introduced. Finally, sample problems were solved to demonstrate the feasibility and potential usefulness of the methodology as a design tool.

The results of the sample problem revealed distinct characteristics of the presented formulations. The multiple-objective formulation provided a solution with acceptable actuator utilization and shape error values. It is observed that the formulation has a characteristic of minimizing both actuator utilization and shape error proportionally as defined by its objective weight constants. This formulation is ideal if both actuator minimization and shape achievements are considered critical in the design. The actuator utilization minimization formulation provided a solution with a less accurate shape and a superior actuator utilization value. It was noted that the actuator minimization formulation is beneficial if the precise shape target achievement is not as important as the actuator minimization. The combination scheme seems to possess an advantage in terms of solution controllability. The sequential solution of the shape or multiple-objective formulations followed by the actuator formulation has the benefit of further minimizing the actuator utilization, provided that the shape errors within the defined shape boundaries are acceptable. The aforementioned differences in the characteristics of formulations may benefit one formulation from another in a certain problem. In other words, each formulation has its unique characteristics and it is premature to state which of these formulations works the best for any given instances. One must decide which formulation might provide the benefit to his/her particular

Table 1 Comparison of solutions from various problem formulations

Formulation	Quantity				
	Push actuator	Pull actuator	Truss	Pin attachment	Sliding attachment
Multi-objective	14	3	30	1	4
Actuator minimize	11	0	33	1	4
Shape error minimize	14	3	33	1	4
Combination multi-objective/actuator	12	3	32	1	4
Combination shape error/actuator	12	3	33	1	4

problem according to design requirements. A summary of the results obtained from various problem formulations is provided in Table 1.

Although more investigations are required to further validate the methodology, it is sufficiently demonstrated via a sample in-plane morphing problem that the methodology presented in this paper may provide a viable solution. In addition, future investigation must include an out-of-plane scheme to handle aerodynamic pressure loads along with coupled aeroelastic formulations. Although numerous simplifications were made in this paper, it is the authors' impression that this preliminary investigation serves as important evidence that the methodology, with extensions and improvements, can potentially be used for the determination of practicable morphing aircraft structures.

Acknowledgments

The authors would like to thank Krister Svanberg of Royal Institute of Technology, Stockholm, for providing his optimization code and educational materials. Also, the authors would like to acknowledge the support by Dayton Area Graduate Studies Institute and the U.S. Air Force Office of Scientific Research.

References

- [1] Kudva, J., "Overview of the DARPA Smart Wing Project," *Journal of Intelligent Material Systems and Structures*, Vol. 15, No. 4, 2004, pp. 261–267.
- [2] Bowman, J., Sanders, B., and Weisshaar, T., "Identification of Military Morphing Aircraft Missions and Morphing Technology Assessment," SPIE Paper 4698-62, 2002, pp. 121–132.
- [3] Maute, K., Reich, G., and Sanders, B., "In-Plane Morphing Designs by Topology Optimization," *16th International Conference of Adaptive Structures and Technologies*, DEStech Publications, Lancaster, PA, 2006, pp. 291–300.
- [4] Maute, K., and Reich, G., "Integrated Multidisciplinary Topology Optimization Approach to Adaptive Wing Design," *Journal of Aircraft*, Vol. 43, No. 1, 2006, pp. 253–263.
- [5] Lu, K.-J., and Kota, S., "Design of Compliant Mechanisms for Morphing Structural Shapes," *Journal of Intelligent Material Systems and Structures*, Vol. 14, No. 6, 2003, pp. 379–391.
- [6] Gern, F. H., Inman, D. J., and Kapania, R. K., "Structural and Aeroelastic Modeling of General Planform Wings with Morphing Airfoils," *AIAA Journal*, Vol. 40, No. 4, 2002, pp. 628–637.
- [7] Prock, B., Weisshaar T. A., and Crossley, W. A., "Morphing Airfoil Shape Change Optimization with Minimum Actuator Energy as an Objective," AIAA Paper 2002-5401, 2002.
- [8] Sanders, B., Reich, G., Joo, J., and Eastep, F., "Air Vehicle Control Using Multiple Control Surfaces," AIAA Paper 2004-1887, 2004.
- [9] Austin, F., Rossi, M. J., Van Nostrand, W., and Knowles, G., "Static Shape Control for Adaptive Wings," *AIAA Journal*, Vol. 32, No. 9, 1994, pp. 1895–1901.
- [10] Cook, A., and Crossley, W. A., "Genetic Algorithm Approaches to Smart Actuator Placement for Aircraft Flight Control," AIAA Paper 2000-1582, 2000.
- [11] Mattingly, M., Roemer, R. B., and Devasia, S., "Optimal Actuator Placement for Large Scale Systems: A Reduced-Order Modeling Approach," *International Journal of Hyperthermia*, Vol. 14, No. 4, 1998, pp. 331–345.
- [12] Liang, C., Sun, F. P., and Rogers, C. A., "Determination of Design of Optimal Actuator Location and Configuration Based on Actuator Power Factor," *Journal of Intelligent Material Systems and Structures*, Vol. 6, No. 4, 1995, pp. 456–464.
- [13] Frecker, M., Ananthasuresh, G., Nishiwaki, G., Kikuchi, N., and Kota, S., "Topological Synthesis of Compliant Mechanism Using Multi-Criteria Optimization," *Journal of Mechanical Design*, Vol. 199, No. 2, 1997, pp. 238–245.
- [14] Pedersen, C. B. W., Buhl, T., and Sigmund, O., "Topology Synthesis of Large-Displacement Compliant Mechanisms," *International Journal for Numerical Methods in Engineering*, Vol. 50, No. 12, 2001, pp. 2683–2705.
- [15] Joo, J.-J., Sanders, B., and Washington, G., "Energy Based Efficiency of Adaptive Structures Systems," *Smart Materials and Structures*, Vol. 15, No. 1, 2006, pp. 171–181.
- [16] Svanberg, K., "The Method of Moving Asymptotes—A New Method for Structural Optimization," *International Journal for Numerical Methods in Engineering*, Vol. 24, No. 2, 1987, pp. 359–373.
- [17] Svanberg, K., "A Globally Convergent Version of MMA Without Line Search," *Proceedings of the First World Congress of Structural and Multidisciplinary Optimization*, Pergamon, Elmsford, NY, 1995, pp. 9–16.